Colloquia: LaThuile15

Heavy quark physics in CMS

G. Fedi on behalf of the CMS Collaboration

INFN, Sezione di Pisa - Pisa, Italy

Summary. — The most recent results which concern the heavy quark hadrons done in the CMS experiment are reported. The searching area spans over the heavy quark spectroscopy, production cross sections, beauty meson decay properties, rare decays, and CP violation.

PACS `14.40.Pq` – Heavy quarkonia.

1. – Introduction

Recent results regarding the heavy quark physics in CMS [1] can be divided in two main categories: the indirect search for new physics beyond the Standard Model and the study of charm and beauty hadrons production and decay. In the former analysis category a measurement which lead to a different results from the Standard Model expectation, gives the hint that new physics might be present in the measured processes, see sect. **2** and **3**. While in the latter category, the analyses aim is to do precise measurements within the Standard Model framework, or aim to test the theoretical approximations of the studied process, see sect. **4**, **5**, **6**. **7**, **8** and **9**.

2. – Search for $B_{(s,d)} \to \mu\mu$

The rare decays $B_s \to \mu\mu$ and $B_d \to \mu\mu$ were studied combining the CMS data collected at the center-of-mass energy of $\sqrt{s} = 7$ and 8 TeV for a total integrated luminosity of 5 and 20 fb^{-1}, respectively [2].

The aim of the studies was to search for events of those two rare decays. In case of no evidence of signal were found new production upper limits would have been set. In the Standard Model of particle physics the $B_{(s,d)} \to \mu\mu$ decays are highly suppressed since they cannot decay through the tree-level diagrams. The flavour changing neutral-current FCNC transitions are only possible via box or penguin diagrams, see fig. 1. Furthermore the decays are Cabibbo and helicity suppressed. The Standard Model predictions for the branching fraction are $\mathcal{B}(B_s \to \mu\mu) = (3.66 \pm 0.23) \cdot 10^{-9}$ and $\mathcal{B}(B_d \to \mu\mu) = (1.06 \pm 0.10) \cdot 10^{-10}$ [3]. Any measured deviation of the branching fractions with respect
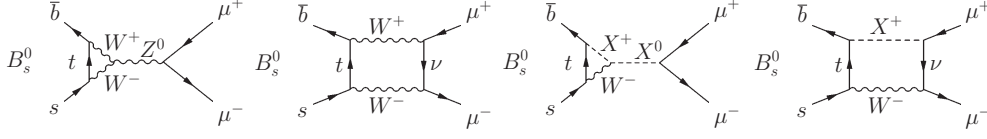
Fig. 1. – $B_s \to \mu\mu$ decay Feynman diagrams. From left to right: SM penguin diagram, SM box diagram, new physics penguin diagram, and new physics box diagram.

to the Standard Model prediction might be a hint of New Physics particles present in box or penguin diagrams, see fig. 1.

With an unbinned maximum-likelihood fit to the dimuon invariant mass distribution the branching fraction $\mathcal{B}(B_s \to \mu\mu) = (3.0^{+0.9}_{-0.8}(\text{stat.})^{+0.6}_{-0.4}(\text{syst.})) \cdot 10^{-9}$ is measured. An excess of $B_s \to \mu\mu$ events with respect to background is observed with a significance of 4.3 standard deviations. In case of the decay branching ratio $\mathcal{B}(B_d \to \mu\mu) < 1.1 \cdot 10^{-9}$, an upper limit is determined at 95% of confidence level. Both results are in agreement with the expectations from the standard model. The two-dimensional likelihood scan of the fit is shown in fig. 2.

3. – CP-violating phase ϕ_s using $B_s \to J/\psi\phi(1020)$ channel

The CP-violating weak phase ϕ_s and the decay width difference $\Delta\Gamma_s$ of B_s meson are measured by the CMS experiment at the LHC using a data sample of $B_s \to J/\psi\phi(1020)$ decays [4]. The analysed data sample corresponds to an integrated luminosity of $20\,\text{fb}^{-1}$ collected in pp collisions at $\sqrt{s} = 8\,\text{TeV}$.

The weak phase ϕ_s of B_s arise from the interference between direct B_s meson decays into a CP eigenstate and decays through mixing to the same final state. It is predicted by the mean of a global fit of the SM parameters to be $\phi_s = 0.0363^{+0.0016}_{-0.0015}$ rad [5].
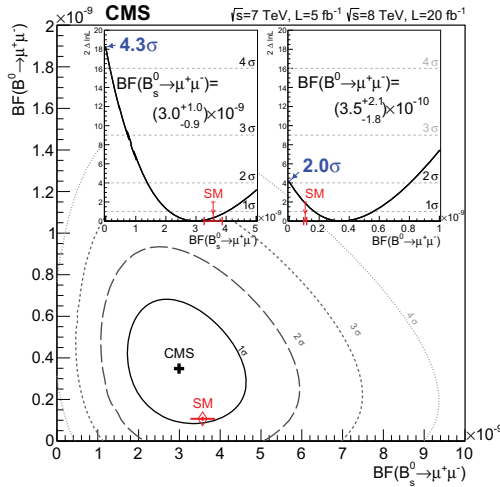

Fig. 2. – Two-dimensional likelihood scan for $\mathcal{B}(B_s \to \mu\mu)$ and $\mathcal{B}(B_d \to \mu\mu)$. The red point shows the SM prediction value.
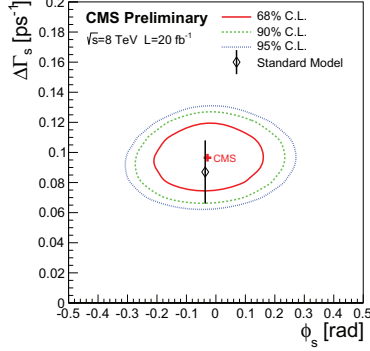
Fig. 3. – Two-dimensional scan of the likelihood function for ϕ_s and $\Delta\Gamma_s$, the best fit values and the C.L. contours are shown in comparison with the SM prediction.

Being the predicted ϕ_s with a good accuracy and close to zero, a significant deviation of the measured weak phase with respect to the prediction, might be the sign of NP particles in the mixing decay of B_s.

An angular analysis of the B_s decay based on three angles (θ_T, ψ_T, and ϕ_T) is needed in order to disentangle the two CP states (odd and even). The differential decay rate of B_s is studied in terms of proper decay time and the angular variables. In order to increase the sensitivity on ϕ_s, the flavour of B_s at production time (flavour tagging) is used as an observable in the fit of data. The total tagging power of tagging is $(0.97 \pm 0.03)\%$.

Assuming a polarisation-independent CP violation model and no direct CP violation, the values for the weak phase and the decay width difference between the B_s mass eigenstates are measured to be:

$$\phi_s = -0.03 \pm 0.11 \text{ (stat)} \pm 0.03 \text{ (syst) rad},$$

$$\Delta\Gamma_s = 0.096 \pm 0.014 \text{ (stat)} \pm 0.007 \text{ (syst) ps}^{-1}.$$

In fig. 3 the two-dimensional scan of the likelihood function for ϕ_s and $\Delta\Gamma_s$ is shown. The value of ϕ_s is in statistical agreement with the SM fit prediction. The $\Delta\Gamma_s$ is confirmed to be non-zero.

4. – $B^+ \rightarrow \psi(2S)\phi K^+$ rare decay

The $B^+ \rightarrow \psi(2S)\phi K^+$ invariant mass peak was detected by the CMS experiment using 19.6 fb^{-1} integrated luminosity at $\sqrt{s} = 8 \text{ TeV}$ of center-of-mass energy. The unbinned maximum likelihood fit was performed on the invariant mass distribution to extract the peak characteristics. The likelihood function is composed by the signal PDF, which is parametrized as a double Gaussian. While the background PDF is parametrized as a first-order Chebyshev polynomial. In fig. 4 the mass distribution and the best fit projection is shown. The peak centroid is compatible with the B^+ mass and the measured resolution is about 3 MeV. The obtained signal events might be used to measured the $B^+ \rightarrow \psi(2S)\phi K^+$ decay branching fraction.
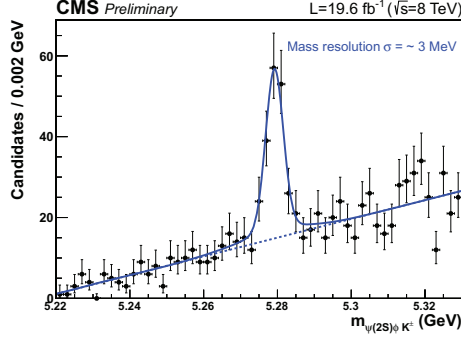
Fig. 4. – $B^+ \to \psi(2S)\phi K^+$ invariant mass distribution and relative best fit. The lines represent the signal-plus-background fit (solid) and the background-only component (dashed).

5. – B_c decays

At a center-of-mass energy $\sqrt{s} = 7$ TeV in proton-proton collisions, the ratio of the production cross sections times branching fractions $\sigma(B_c^{\pm}) \times \mathcal{B}(B_c^{\pm} \to J/\psi\pi^{\pm})/\sigma(B^{\pm}) \times \mathcal{B}(B^{\pm} \to J/\psi K^{\pm})$ is studied [6]. The analysed data sample corresponds to an integrated luminosity of $5.1\,\mathrm{fb}^{-1}$. The ratio is determined to be $(0.48 \pm 0.05(\mathrm{stat}) \pm 0.03(\mathrm{syst}) \pm 0.05(\tau_{B_c})) \times 10^{-2}$ in the kinematic region that requires $B_c^{\pm}$ and $B^{\pm}x$ mesons with transverse momentum $p_{\mathrm{T}} > 15$ GeV and rapidity $|y| < 1.6$. A previous measurement of the same ratio done by LHCb is in agreement with the present result taking into account for the different kinematic regions used in the analyses.

The ratio of the branching fractions $R = \mathcal{B}(B_c^{\pm} \to J/\psi\pi^{\pm}\pi^{\pm}\pi^{\mp})/\mathcal{B}(B_c^{\pm} \to J/\psi\pi^{\pm})$ is also measured. The efficiencies were assessed using a model-independent method. The measured ratio is $R = 2.55 \pm 0.80(\mathrm{stat}) \pm 0.33(\mathrm{syst})^{+0.04}_{-0.01}(\tau_{B_c})$, consistent with the previous LHCb result.

In figs. 5 the invariant mass distributions for $B_c^{\pm} \to J/\psi\pi^{\pm}\pi^{\pm}\pi^{\mp}$ (left) and $B_c^{\pm} \to J/\psi\pi^{\pm}$ (right) are shown.
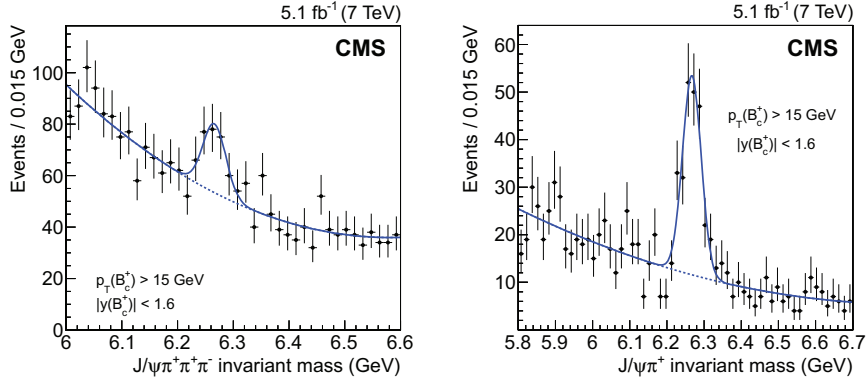

Fig. 5. – Invariant mass distributions for $B_c^{\pm} \to J/\psi\pi^{\pm}\pi^{\pm}\pi^{\mp}$ (left) and $B_c^{\pm} \to J/\psi\pi^{\pm}$) (right). The fit function projections is also shown.
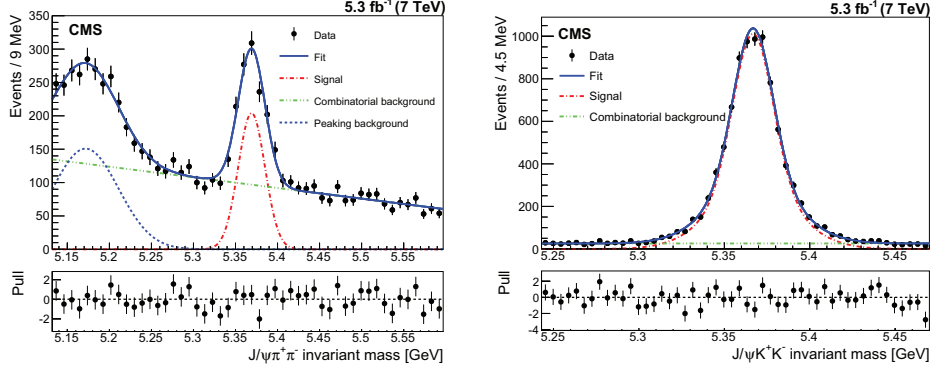
Fig. 6. – Invariant mass distributions for $B_s \to J/\psi f_0(980)$ (left) and $B_s \to J/\psi\phi(1020)$ (right). The fit function projections is also shown.

6. – $\mathcal{B}(B_s \to J/\psi f_0(980))/\mathcal{B}(B_s \to J/\psi\phi(1020))$ ratio

At a centre-of-mass energy of $\sqrt{s} = 7\,\text{TeV}$ in proton-proton collisions, the ratio of branching fractions $R_{f_0/\phi} = \mathcal{B}(B_s \to J/\psi f_0(980))/\mathcal{B}(B_s \to J/\psi\phi(1020))$ is measured [7]. The analysed data sample corresponded to an integrated luminosity of $5.3\,\text{fb}^{-1}$. The measured ratio is $R_{f_0/\phi} = 0.140 \pm 0.013(\text{stat}) \pm 0.018(\text{syst})$, where the first uncertainty is statistical and the second is systematic. This result is consistent with theoretical predictions and previous measurements.

In figs. 6 the invariant mass distributions for $B_s \to J/\psi f_0(980)$ (left) and $B_s \to J/\psi\phi(1020)$ (right) are shown.

7. – J/ψ and $\psi(2S)$ production

At a centre-of-mass energy of $\sqrt{s} = 7\,\text{TeV}$ in proton-proton collisions, the double-differential cross sections of promptly produced J/ψ and $\psi(2S)$ mesons are measured as a function of transverse momentum p_T and absolute rapidity $|y|$ [8]. The analysed J/ψ and $\psi(2S)$ data samples correspond to integrated luminosities of 4.55 and $4.90\,\text{fb}^{-1}$, respectively. The differential cross section as a function of p_T only, where the rapidity is integrated for values lower than 1.2, is also measured. With the present analysis the highest-p_T values in the context of the measured cross sections has been reached.

In figs. 7 we show the differential cross sections as a function of p_T times the dimuon branching fractions for four rapidity bins and integrated over the range $|y| < 1.2$ (left) and the J/ψ and $\psi(2S)$ differential cross sections integrated over rapidity (right).

8. – $\Upsilon(nS)$ production

At a centre-of-mass energy of $\sqrt{s} = 7\,\text{TeV}$ in proton-proton collisions, the differential cross sections as a function of transverse momentum p_T for the production of $\Upsilon(nS) \to \mu\mu$ ($n = 1, 2, 3$) are presented [9]. The analysed data samples correspond to integrated luminosities of $4.9\,\text{fb}^{-1}$. The $\Upsilon(nS)$ candidates are selected from those with dimuon rapidity $|y| < 1.2$ and transverse momentum $10 < p_T < 100\,\text{GeV}$.

This measure extends the maximum p_T range from 70 to $100\,\text{GeV}$ with respect the previous results. The measurements show a transition from an exponential to a power-law
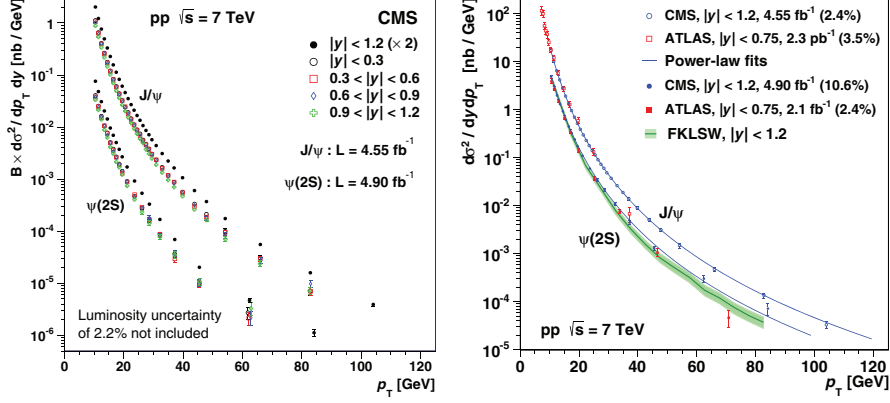
Fig. 7. – Left: J/ψ and ψ(2S) the differential cross sections as function of p_T times the dimuon branching fractions for four rapidity bins and integrated over the range $|y| < 1.2$. Right: J/ψ and ψ(2S) differential cross sections integrated over rapidity.

behavior at pt 20 GeV for the three Υ states. In figs. 8 we show: the $\mu\mu$ invariant mass distribution and the well definite $\Upsilon(nS)$ peaks (left) and the relative differential cross sections as a function of p_T (right).

9. – χ_{bn} production

At a centre-of-mass energy of $\sqrt{s} = 8$ TeV in proton-proton collisions, the production cross section ratio $\sigma(\chi_{b2})/\sigma(\chi_{b1})$ is presented [10]. The analysed data samples correspond to integrated luminosities of 20.7 fb^{-1}.

The prompt $\chi_{b1}(1P)$ and $\chi_{b2}(1P)$ are detected using the radiative decays $\chi_{b1,2}(1P)\rightarrow\Upsilon(1S)+\gamma$. The emitted photons are reconstructed using the decay to electron pairs while interacting with the tracker material (converted photons). That permitted the $\chi_{b1,2}(1P)$ peaks to be resolved. The selected $\chi_{b1,2}(1P)$ kinematic region is defined by the photon pseudorapidity $|\eta| < 1.0$, the $\Upsilon(1S)$ rapidity $|y| < 1.5$, and the $\Upsilon(1S)$ transverse momentum $7 < p_T < 40$ GeV.
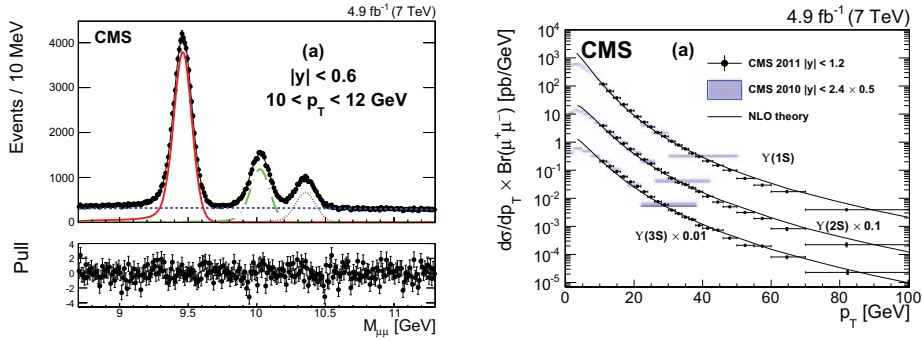

Fig. 8. – Left: $\mu\mu$ invariant mass distribution and best fit projections. Right: the $\Upsilon(nS)$ differential cross sections as a function of p_T.
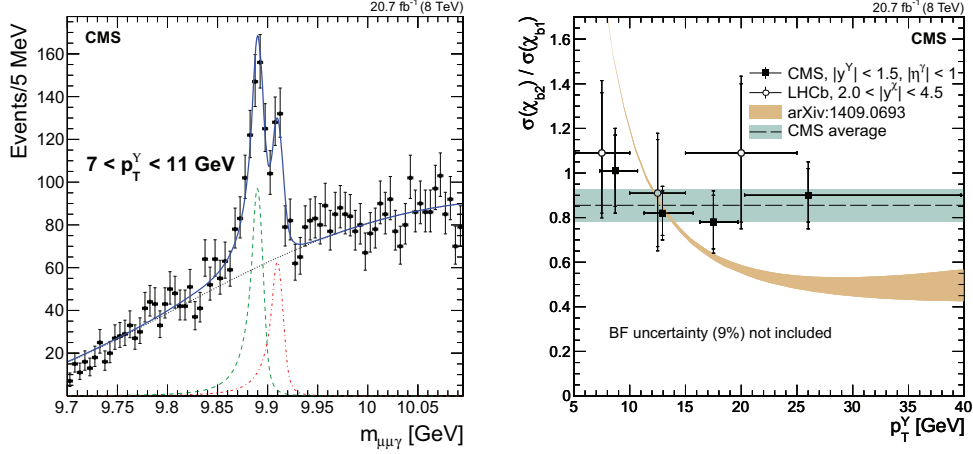
Fig. 9. – Left: $\mu\mu\gamma$ invariant mass distribution of the $\chi_{b1,2}(1P)$ peaks and fit function projections for the first Υ rapidity bin. Right: cross sections ratio $\sigma(\chi_{b2})/\sigma(\chi_{b1})$ as a function of the $\Upsilon(1S)$ p_T.

The cross section ratio is measured as function of $\Upsilon(1S)$ transverse momentum. The measured average value of the cross section is $0.85 \pm 0.07(\text{stat} + \text{syst}) \pm 0.08\ (\text{BF})$, where the first uncertainty is the combination of the statistical and systematic uncertainties and the second is due to the uncertainty of the branching fractions.

In figs. 9 we show: the $\mu\mu\gamma$ invariant mass distribution of the $\chi_{b1,2}(1P)$ peaks for the first Υ rapidity bin (left) and the relative cross sections ratio as a function of the $\Upsilon(1S)$ p_T (right). The cross section ratio does not shows any significant dependence on the $\Upsilon(1S)$ transverse momentum.

REFERENCES

[1] CMS COLLABORATION, *JINST*, **3** (2008) S08004.
[2] CHATRCHYAN S. *et al.* (CMS COLLABORATION), *Phys. Rev. Lett.*, **111** (2013) 101804, arXiv:1307.5025 [hep-ex].
[3] BOBETH C., GORBAHN M., HERMANN T., MISIAK M., STAMOU E. and STEINHAUSER M., *Phys. Rev. Lett.*, **112** (2014) 101801, arXiv:1311.0903 [hep-ph].
[4] CMS COLLABORATION, CMS-PAS-BPH-13-012.
[5] CHARLES J., DESCHAMPS O., DESCOTES-GENON S., ITOH R., LACKER H., MENZEL A., MONTEIL S. and NIESS V. *et al.*, *Phys. Rev. D*, **84** (2011) 033005, arXiv:1106.4041 [hep-ph].
[6] KHACHATRYAN V. *et al.* (CMS COLLABORATION), *JHEP*, **01** (2015) 063, arXiv:1410.5729 [hep-ex].
[7] (CMS COLLABORATION), submitted to *Phys. Lett. B*, arXiv:1501.06089 [hep-ph].
[8] KHACHATRYAN V. *et al.* (CMS COLLABORATION), *Phys. Rev. Lett.*, **114** (2015) 191802, arXiv:1502.04155 [hep-ph].
[9] KHACHATRYAN V. *et al.* (CMS COLLABORATION), *Phys. Lett. B*, **749** (2015) 14, arXiv:1501.07750 [hep-ph].
[10] KHACHATRYAN V. *et al.* (CMS COLLABORATION), *Phys. Lett. B*, **743** (2015) 383, arXiv:1409.5761 [hep-ph].